Surface modification of natural porous silica microparticles to control the loading and release of organic corrosion inhibitors in coatings

Zhao, Jingjing; Na, Dong Hyuk; Garcia, Santiago J.

DOI
10.1038/s41427-025-00608-5

Publication date
2025

Document Version
Final published version

Published in
NPG Asia Materials

Zhao et al. *NPG Asia Materials* (2025)17:27
https://doi.org/10.1038/s41427-025-00608-5

NPG Asia Materials

ARTICLE Open Access

Surface modification of natural porous silica microparticles to control the loading and release of organic corrosion inhibitors in coatings

Jingjing Zhao[1], Dong-Hyuk Na[1] and Santiago J. Garcia[1]

Abstract

Recent works have shown the potential of diatomaceous earth (DE) as an efficient and environmentally friendly storage system for active chemicals such as corrosion inhibitors in coatings. The storage of organic inhibitors is nevertheless challenging. To address this challenge, in this work, we study the effect of surface modification of DE particles on the loading and release of organic corrosion inhibitors in solution and from coatings. To this aim, three trichlorosilanes with varying alkyl chain lengths (C4, C8, C18) were used to modify the surface of sp. *Aulacoseira*-type diatomite (DE). 2,5-Dimercapto-1,3,4-thiadiazolate di-potassium salts (KDMTD) were selected as a model corrosion inhibitor for its high solubility and effectiveness in protecting Cu-rich aerospace alloys, such as AA2024-T3. UV-Vis spectroscopy revealed a relationship between chain length and inhibitor loading and release, with mid-length silane (C8) adsorbing 3.5 times more inhibitor with no negative effect on release kinetics. When incorporated into epoxy-amine coatings, C8 surface modification significantly improved DE particle dispersion and protection of the inhibitor from the polymer matrix, preventing unwanted side reactions. This increased the availability of active organic inhibitors for protection at damaged sites. In-situ reflected microscopy during immersion and postmortem analysis of damaged coatings demonstrated high levels of corrosion protection and the formation of stable protective layers at damaged sites. The research opens the path to more efficient use of functional DE particles in coatings.

Introduction

Incorporating corrosion inhibitors in organic coatings is a widely used strategy to protect metallic surfaces from corrosion induced by environmental conditions (e.g., electrolyte, pH, temperature)[1–3]. Among corrosion inhibitors, organic corrosion inhibitors are promising alternatives to inorganic inhibitors containing toxic or critical elements such as Cr(VI), Li and Rare Earths (RE)[4–6] used to protect aerospace aluminium alloy structures, amongst others. Even though many organic inhibitors show excellent intrinsic corrosion inhibition efficiency in solution, relatively low toxicity and low molecular weight[7,8], their integration in sufficiently high amounts into organic coatings without unwanted reactions remains challenging[9–11].

Inhibitor storage in nano, and to a lower extent, micro-sized inorganic particles has been explored to prevent negative interactions and provide on-demand inhibitor release[12–14]. Nanocarriers such as nanotubes[15], nanofibers[16], layered double hydroxide (LDH)[17], and mesoporous silica[18] provide good dispersion and protection for inhibitors. However, the relatively low loading of inhibitors in nanocarriers and the relatively low CPVC of nanoparticles in coatings limit the use of the nanocarriers and their efficiency for long-term protection at relatively large damages (e.g. >100 µm wide)[10,19]. In contrast, microcarriers such as $CaCO_3$[20] and diatomaceous earth microparticles or diatomite (DE)[21,22] provide the potential of higher loading and long-term protection against larger damages. DE microparticles offer very attractive opportunities as they are readily available as mining products and are currently used as fillers in coatings due to their innocuous amorphous silica composition and price, amongst other properties. In our previous works, we

Correspondence: Jingjing Zhao (J.Zhao-6@tudelft.nl) or Santiago J. Garcia (s.j.garciaespallargas@tudelft.nl)
[1]Aerospace Structures and Materials Department, Faculty of Aerospace Engineering, Delft University of Technology, Delft 2629 HS, The Netherlands

demonstrated the potential of these DE particles as carriers of inorganic salts (Ce-salts), leading to very high corrosion inhibition levels at large damaged locations during immersion[21,22] and explored their potential as carriers of 2,5-Dimercapto-1,3,4-thiadiazole (HDMTD), a highly effective corrosion inhibitor[23]. Nevertheless, when loaded in DE particles embedded in an epoxy coating, HDMTD showed limited protection at damage locations. This was related to (i) a very low loading below 2% of the available internal volume of DE particles, and (ii) side reactions with the organic matrix or the coating leading to reduced release[21].

The effect of surface modification of silica particles, such as nanoparticles and diatomaceous earth (DE) microparticles, has been investigated for their use as fillers to improve the mechanical properties of polymeric matrices and as carriers for drug delivery in solution[24,25]. Among the different approaches, increased loading capacity of drugs using DE has been shown after modifying the surface with opposite water affinities (i.e., hydrophobicity) to the silica surface and/or surface charge balance between carrier and drug[26,27]. Despite significant differences in molecular structure and size, organic corrosion inhibitors and drugs are somewhat similar in terms of water solubility and the presence of certain reactive functional groups (e.g., amines, thiols). However, unlike drugs, corrosion inhibitors used in coatings must be evenly distributed in organic matrices while remaining isolated to avoid unwanted side chemical reactions. They must also retain their activity for long periods of time (years), dissolve quickly but not too quickly to prevent blistering and fast depletion, amongst others, and be transported from the coating to a damage location to react with the exposed metal surface in adequate quantities. These requirements pose an extra challenge when dealing with organic inhibitors in DE microparticles beyond loading and release challenges in aqueous solutions typically faced in drugs.

In this work, we studied how and to what extent alkyl chains of different lengths and their hydrophobic nature can affect the loading and release of an organic corrosion inhibitor from DE microparticles in solution and in a reactive coating. To this aim, we chose 2,5-Dimercapto-1,3,4-thiadiazolate di-potassium salts (KDMTD), a hygroscopic organic inhibitor of relevance for Cu-rich aluminium structures yet difficult to load in DE particles and resins without side reactions. To control the surface hydrophobicity of the DE and the surface wettability difference with the hydrophilic organic inhibitor, three hydrophobic silanes with varying chain lengths (C4, C8, and C18) were selected. The modified DE particles exhibiting the most optimal combination of high loading and release kinetics and efficiency were further embedded into a prototype epoxy-amine coating and applied onto aerospace-grade AA2024-T3. The coating properties, including aspects like pigment distribution, resin penetration into pigments, and release kinetics, were evaluated using confocal microscopy, scanning electron microscopy (SEM), energy-dispersive X-ray spectroscopy (EDS), and UV/Vis spectroscopy. Additionally, the corrosion inhibition efficiency and inhibitor layer stability at damaged locations were investigated by exposing the damaged coating to NaCl electrolytes and monitored and quantified using an in-situ, high-resolution image reflectometry set-up and image treatment protocols.

Experimental

Materials

Diatomaceous earth (DE) DiaFil525 particles were supplied by Profiltra Customized Solutions. A cleaning protocol using the decantation principle in water was used to maximize the content of intact DE particles, as reported earlier[21,22]. Commercial-grade bare AA2024-T3 (2.5 mm thick rolled sheets) were cut into 3 × 3 cm pieces and used as the substrate for the coated panels. 2,5-dimercapto-1,3,4-thiadiazolate di-potassium salts (KDMTD > 99%), Butyl trichlorosilane (BTS), Octyl trichlorosilane (OTS) and Octadecyl trichlorosilane (ODTS) (>97%), and hydrogen peroxide (30%) were purchased from Sigma-Aldrich and used without further purification. Sodium chloride (NaCl, >98%), ethanol (>99.9%), anhydrous toluene (>99.85%), and toluene (>98%) were purchased from VWR Chemicals and used as received.

Surface modification of DE particles

Firstly, the cleaned DE particles were hydrolyzed to increase the content of active hydroxyl sites for silanization as reported elsewhere[28]. Specifically, 10 g of cleaned DE particles were dispersed in 30 ml of 30 wt% hydrogen peroxide in water and sonicated for 10 min. The sonicated dispersion was refluxed at 90 °C for 3 h in N_2. DE particles were collected using Whatman® filter paper grade 595 (pore size 7 µm) with vacuum suction. The DE particles residue collected at the filter was dried at 80 °C for 6 h, removed from the filter and stored in a glass vial.

After hydroxylation, the DE particles were modified with three different hydrophobic silanes using the following silanization protocol based on a previously reported protocol[26]: (i) DE particles were dried in nitrogen at 150 °C for 15 h; (ii) 0.5 g of DE particles were dispersed in 20 ml of anhydrous toluene and stirred using magnetic stirring for 30 min; (iii) A solution composed of 16 ml of toluene and 4 ml silane was added dropwise to the dispersion prepared in (ii) while stirring. After 15 min stirring, the dispersion was refluxed at 150 °C for 24 h in a nitrogen atmosphere. After 24 h, the solution was let to cool down to room temperature for 2 h; (iv) The modified DE particles were collected using Whatman® filter paper

grade 595 with vacuum suction; (v) The DE particles collected residue was scrapped from the filter and sonicated in 30 ml of ethanol for 5 min to remove residual silane; (vi) The modified DE particle dispersion in ethanol was then filtered using Whatman® filter paper grade 595 with vacuum suction. The steps (v) and (vi) were repeated twice to finally dry the collected modified DE particles residue in a vacuum at 80 °C for 4 h and stored in a vial.

The same procedure, with or without silane, was repeated to obtain DE particles with four surface treatments: cleaned and hydrolyzed (DE), silanized with BTS (C4@DE), silanized with OTS (C8@DE), and silanized with ODTS (C18@DE).

Loading of organic corrosion inhibitors in DE

Figure 1 shows the loading protocol of KDMTD organic corrosion inhibitor inside the (modified) DE particles. The inhibitor loading process consisted of the following sequential steps shown in Fig. 1:

Step 1: KDMTD was dissolved in demineralized water under magnetic stirring to create a 0.5 M KDMTD aqueous solution. This defines c_1 and m_1;

Step 2: 0.5 g DE particles (m_{DE}), with/without surface modification, were added to 20 mL 0.5 M KDMTD aqueous solution in a glass jar and stirred with a high-speed mixer for 5 min. After this, the dispersions were transferred to a stirring table and kept stirring for 24 h at 300 rpm;

Step 3: The dispersions were centrifuged at 4000 rpm for 10 min for separation;

Step 4: The supernatant solution on top of the densely packed DE particles was removed with a glass pipette and collected in a separate vial to measure the unloaded KDMTD concentration (c_2) and mass ($m_u=m_1-m_{LO}$). The separated DE particles with leftover solution was weighted with a balance to obtain $m=m_{LO}+m_{DE}$, where the m_{DE} is the original mass of DE added, allowing to calculate m_{LO};

Step 5: The vial with the DE cake obtained from centrifugation was then moved to a vacuum oven at 70 °C for 6 h to evaporate the remaining water. The inhibitor-loaded DE particles were then collected with a spatula and brought to a smaller vial for storage. After drying, the particles (DE-KDMTD, C4@DE-KDMTD, C8@DE-KDMTD, and C18@DE-KDMTD) appeared as a loose powder not requiring further grinding before further use.

The loading protocol shown above allowed loading and a quantified approximation method to identify the inhibitor loading fraction that is adsorbed and absorbed in the DE powder, as shown in Fig. 2 and discussed below. Adsorbed KDMTD inhibitor attributed to the attraction forces between DMTD ions and the DE (modified) silica surface during the loading process in solution is depicted by the yellow region in Fig. 2. Absorbed inhibitor, primarily happening during the final drying step, can be subdivided into three different categories[29,30], namely: (i) externally absorbed (green), (ii) internally absorbed (red), and (iii) non-bound (loose) inhibitor salts (purple). When slowly drying the DE cake after centrifuge, most of the

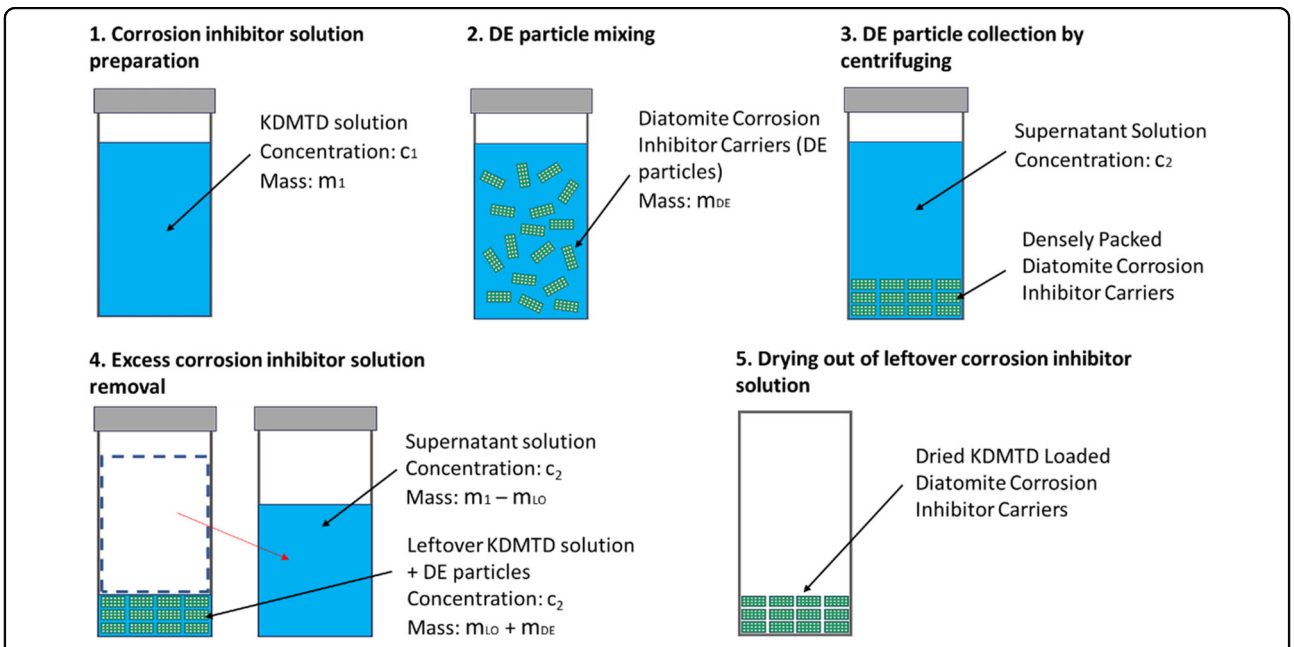

Fig. 1 Protocol to load KDMTD in the (modified) DE particles. This method allows a quantified approximation to identify the inhibitor loading fraction that is adsorbed and absorbed in the carriers, as shown in Fig. 2.

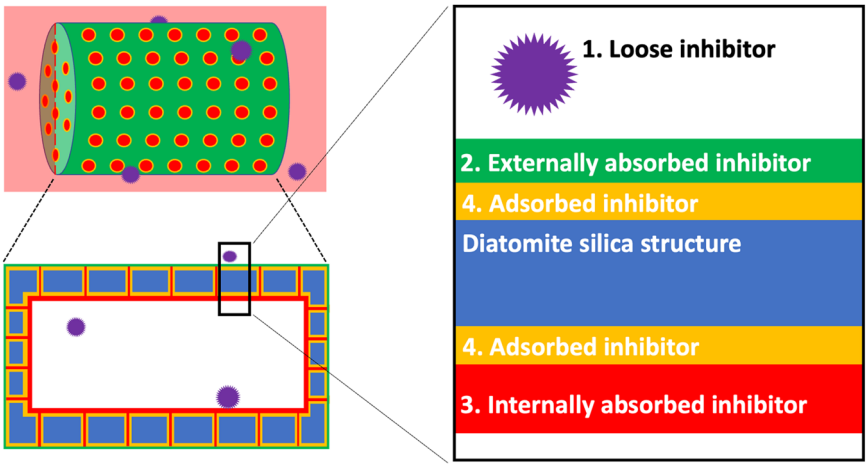

Fig. 2 Idealized diatomite shell particle loaded with corrosion inhibitor. Schematic showing an idealized diatomite shell particle loaded with a corrosion inhibitor and a cross section of the particle with a close up (right drawing) of the shell wall to indicate the different states of the inhibitor in the carriers: adsorbed onto the silica frustule walls (yellow, surface loading), absorbed (red and green being inner and outer shell absorption) and non-bound or loose inhibitor salts mixed with the DE particles (purple).

KDMTD-rich electrolyte retreats to the interior volume of the DE particles, hence allowing local precipitation of KDMTD after concentration increases above the local solubility limit in a constrained space. However, a small portion of electrolyte remained trapped between the particles, leading to inhibitor salt precipitation on the outer surfaces of the DE particles. Besides this, some KDMTD-rich pockets remain trapped between the dry DE particles, leading to non-bound (loose) KDMTD agglomerate salts (purple). The presence of KDMTD in different states in the DE powder is expected to lead to different release mechanisms and kinetics (faster when absorbed or loose, and slower when adsorbed) and can hence be used as a design parameter when using this loading strategy. To calculate the amounts of adsorbed and absorbed inhibitor, the following equations were used:

$$m_{AD} = 1000 * (c_1 - c_2) * m_1 * M_{KDMTD} / \rho_1 \quad (1)$$

where, m_{AD} (mg) is the amount of inhibitor adsorbed, c_1 (mol/L) and m_1(g) are the concentration and mass of the KDMTD solution prepared for the loading process, c_2 (mol/L) is the concentration of KDMTD in the supernatant after the centrifugation, M_{KDMTD} (g/mol) is the molar mass of KDMTD and ρ_1(g/L) is the density of the solution.

and,

$$m_{AB} = 1000 * c_2 * m_{LO} * M_{KDMTD} / \rho_2 \quad (2)$$

where, m_{AB} (mg) is the amount of inhibitor absorbed, c_2 (mol/L) is the concentration of KDMTD in the supernatant after the centrifugation, m_{LO} is the mass of the leftover KDMTD solution filling the inter and intra volume of the densely packed DE particles (cake). We assume that the retention capacity of diatomite for the solution is similar to its absorption capacity for pure water. Ideally, when the diatomite particles are stacked very densely, m_{LO} should be 1.6 times heavier than m_{DE} based on the 160 wt% water absorption capacity mentioned in the datasheet of diatomite particles provided by Profiltra. M_{KDMTD} (g/mol) is the molar mass of KDMTD, and ρ_2(g/L) is the density of the solution.

Particles characterization

The structural integrity of DE before and after surface modification was analysed by SEM-EDS in a JEOL JSM-7500F field emission scanning electron microscope equipped with energy dispersive X-ray spectroscopy. Both secondary electron mode (SEM) and backscattered electron mode (BSE) were used with magnification ranging between ×250 up to ×3000 and voltage of 5.0 kV or 15.0 kV. To reduce electrostatic charging, DE particles were first sputtered with a 15 nm thick gold layer.

The hydrophobic surface modification with BTS, OTS and ODTS hydrophobic silanes was evaluated with FTIR spectroscopy with a wavenumber ranging from 700 up to 4000 cm^{-1} and a wavenumber resolution of 0.5 (cm^{-1}). To construct the final spectrum for each sample, 40 scans were averaged.

The loading and release of the corrosion inhibitor in and out of the DE particles were quantified by UV-Vis spectroscopy using a calibration curve for KDMTD in distilled water and in NaCl aqueous solution, respectively. All the tests were repeated three times. Since the

Table 1 Coating formulations as a function of Epikote™ 828 (phr = parts per hundred epoxy resin in weight), and the calculated inhibiting active component in wt% of the total coating dry weight.

Sample Name	Pigment	DE particles (phr)	Inhibiting active component (phr)	Inhibiting active component (wt.%)	Dry thickness (μm)
Epoxy/DE-KDMTD	DE-KDMTD	26.5	7.2	3.8%	73 ± 5
Epoxy/C8@DE-KDMTD	C8@DE-KDMTD	25.9	7.8	4.1%	73 ± 5

The DE pigment volume concentration (PVC%) was set at 30%. Inhibitingthe active component refers to KDMTD.

corrosion inhibitor solution shows the highest absorbance at 315 nm, this wavelength was used to construct the calibration curve (intensity-concentration) and as an identifier to calculate KDMTD content in solution.

The Inhibitor Loading (I_L) is here defined as the amount of KDMTD (mg) that was loaded in 1 g of diatomite carrier particles. It can be calculated using the following equation:

$$I_L(mg\ KDMTD/1gDE) = (m_{AD} + m_{AB})/m_{DE} \quad (3)$$

Where, m_{AD} (mg) is the amount of inhibitor adsorbed, obtained from Eq. 1, m_{AB} (mg) is the amount of inhibitor absorbed, obtained from Eq. 2, m_{DE} (g) is the mass of the DE particles used for loading.

To calculate the release kinetics from the carriers, 100 mL of H_2O/0.05 M NaCl solution in a glass jar was used as the release medium. The media was stirred with a magnetic stirring table at 400 rpm during the whole duration of the release experiment to homogenize the solutions. For each modified diatomite sample, a Whatman 42 filter paper with the shape of a cone was filled with 10 mg of KDMTD-loaded diatomite particles and submerged in a fresh release medium with the help of a large tweezer holder. Aliquots of 4 ml were taken at given time intervals (2, 4, 6, 8, 10, 15, 20, 25, 30, 40, 50, 60, 90, 120, 150, and 180 minutes) and analyzed using UV-Vis spectroscopy. The aliquots were returned to the release media each time after the UV-Vis measurement. At each time point, the absorbance magnitude was measured at the characteristic peak absorbance wavelength (i.e., 315 nm). With the help of a calibration curve for the selected inhibitor in NaCl, the release kinetics and inhibitor concentration in solution were obtained.

The Inhibitor Release (I_R) is defined as the amount of KDMTD (mg) that can be released from 1 g of DE particles over a specific time. It can be calculated using the following equation:

$$I_R(mg\ KDMTD/1gDE) = c_3 * 226.4 * V/m'_{DE} \quad (4)$$

Where, c_3 (mM) is the concentration of KDMTD released in the release medium at time t, V(l) is the volume of the release medium, m'_{DE} (g) is the mass of DE particles used for release tests.

As a maximum release reference point to calculate release fractions (from 0 no release to 1 full release), a theoretical maximum release was defined as the total amount of KDMTD initially loaded in the DE particles (calculated from Eq. 3).

Preparation of coatings and coated panels

2.5 mm thick bare aerospace-grade aluminium alloys AA2024-T3 metal plates were surface cleaned as follows: (1) grinding with Scotch Brite 3 M in water to remove the native oxide layer; (2) wiping with a paper tissue wet in acetone; (3) immersing in 2 M NaOH for 10 s followed by 30 s rinsing in distilled water and drying with N_2 gas. The coating compositions are shown in Table 1. Briefly, Epikote™ 828, Ancamine® 2500, and xylene (weight ratio of 2.70:1.57:1.06) were mixed in a high-speed mixer at 2500 rpm for 5 minutes. This mixture was then pre-cured at ambient temperature for 15 minutes. Selected DE particles loaded with inhibitors (DE-KDMTD, C8@DE-KDMTD) were introduced by stirring the coating formulation manually for 3 minutes. This mixture was then applied onto AA2024 metal coupons with a spiral bar of 100 μm wet film. Following a 30-minute flash-off period at room temperature, the coatings were cured at 60 °C for 24 hours leading to a coating dry thickness of 73 ± 5 μm. Before inhibitor release and corrosion testing, the coated panels were preserved in a desiccator.

Coatings characterization

The effect of surface treatment on the particle distribution in the as-prepared coatings was evaluated by a Keyence VK-X1000 confocal scanning microscope. The coatings were analysed for a second time after manually wet-grinding up to 4000 grit sanding paper using SEM-EDS.

The release capacity of the coatings containing DE-KDMTD and C8@DE-KDMTD was quantified by grinding the surface of the coatings with a 1000-grit paper for 15 seconds and exposing them to 20 mL 0.05 M NaCl solution in a 1 cm diameter container.

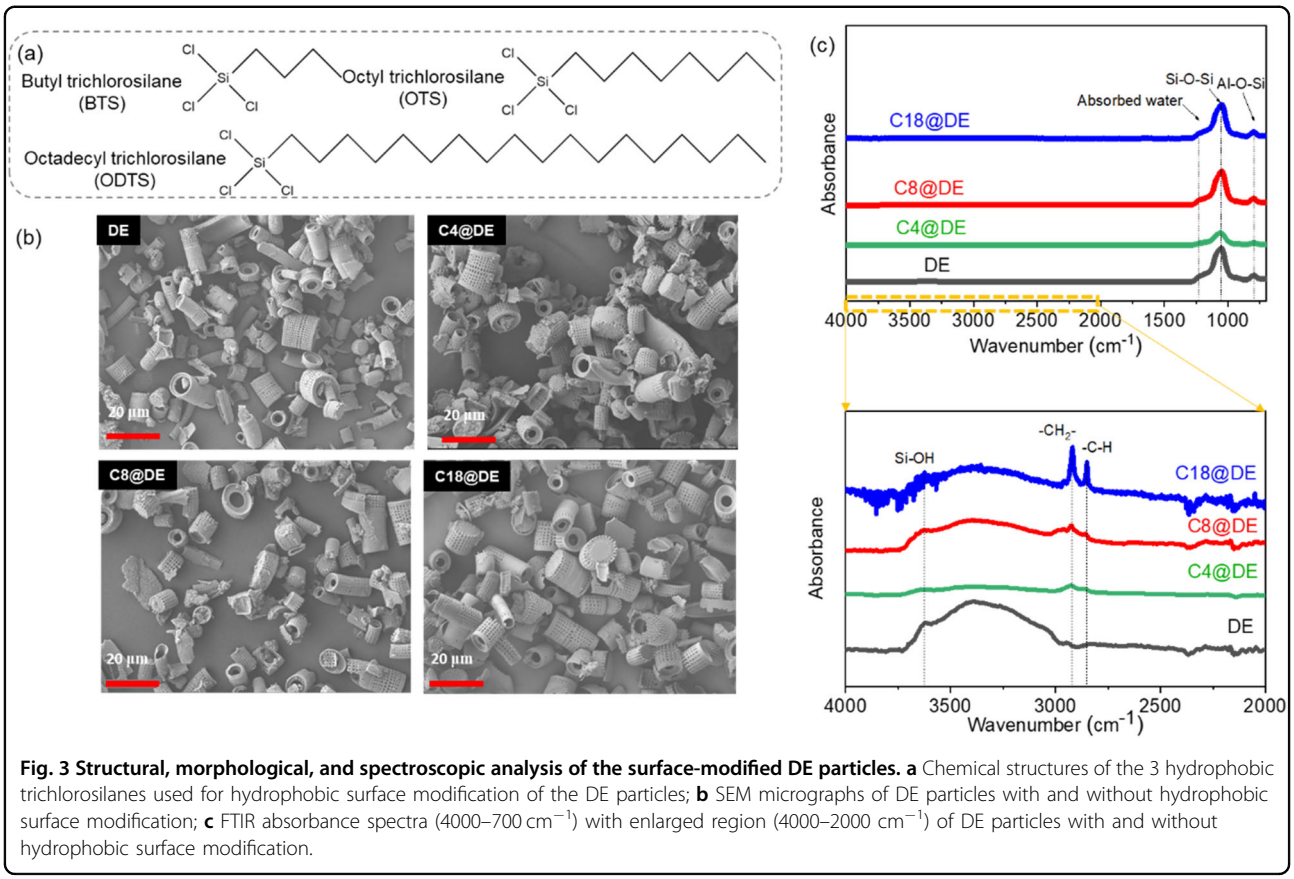

Fig. 3 Structural, morphological, and spectroscopic analysis of the surface-modified DE particles. a Chemical structures of the 3 hydrophobic trichlorosilanes used for hydrophobic surface modification of the DE particles; **b** SEM micrographs of DE particles with and without hydrophobic surface modification; **c** FTIR absorbance spectra (4000–700 cm^{-1}) with enlarged region (4000–2000 cm^{-1}) of DE particles with and without hydrophobic surface modification.

Electrolyte aliquots were measured with a UV-Vis spectrometer using the same calibration curve and wavenumber as shown above to quantify inhibitor release with time. This process allowed direct exposing the loaded particles in the coating to the solution by removing the top thin polymer barrier layer formed during the coating deposition. Aliquots of 3 mL were taken at 1, 5, 15, 30, 60, 120, 240, 360, 1440, and 2880 minutes and returned to the solution to keep the exposure volume constant. A parafilm cover prevented evaporation during the release test. The coating release tests for each sample were repeated three times.

Wet/dry cyclic corrosion inhibition tests

Damages of 1 mm diameter and 0.25 mm deep from the coating surface were performed on the coated panels with the help of a Roland EGX-350 engraver equipped with an end mill carbide tip (1 mm in diameter). The resulting chips were removed by a vacuum cleaner.

The damaged samples were placed in a Raman electrochemical flow cell with 4.5 ml electrolyte and an Ag/AgCl (3 M KCl) reference electrode. This setup was placed vertically on an optical table inside a Faraday cage to avoid electromagnetic and vibrational disturbances. Visualization was achieved through a 150x magnification Dino-Lite digital microscope, positioned adjacent to the viewing window of the cell, thereby enabling the acquisition of high-resolution imagery at one-minute intervals throughout the electrolyte exposure period. Image analysis was performed using ImageJ software, applying a pixel-level correlation method described in our earlier studies[21,22]. To do so, images were processed into 8-bit greyscale, offering 256 levels of intensity from black to white. This approach allows detecting slight surface variations in refractive index affecting the histogram at pixel level (330 nm) produced by corrosion and inhibition processes over time within a specified region of interest (ROI). A static thresholding limit of 10 was used to analyse the metallic surface, to address low-intensity changes, and to optimize signal-to-optical noise ratio without losing relevant information.

After the immersion, the electrolyte solutions were analysed with UV-Vis spectroscopy to quantify the corrosion inhibitor released from the damaged coatings. The damaged-coated panels were finally analysed with a Keyence VK-X1000 confocal scanning microscope at 50x magnification.

Results and discussion

Surface modification of DE using hydrophobic silanes

Figure 3a illustrates the chemical structures of the three hydrophobic silanes (BTS, OTS, and ODTS) used to modify the surface of the DE particles. DE particles modified with BTS, OTS and ODTS are referred to as C4@DE, C8@DE and C18@DE. The cleaned and hydrolyzed DE particle without surface modification is used as reference. Figure 3b shows the SEM images of the DE particles with and without surface modification with hydrophobic silanes, highlighting no detectable effect on particle size distribution (remained between 7 and 15 µm) or particle integrity during the silanization process.

To verify the success of silane modification, FTIR spectroscopy was used. As shown in Fig. 3c for all 4 DE particle samples, the following five main characteristic peaks are visible: (i) a peak at 800 cm^{-1} attributed to the stretching vibration of Al-O-Si[31,32]; (ii) a peak at 1060 cm^{-1} attributed to the asymmetric stretching mode of Si-O-Si bonds; (iii) a peak at 1635 cm^{-1} due to absorbed water[33]; (iv) a shoulder peak at 3619 cm^{-1} due to the surface hydroxyl moieties; and (v) a broadening OH peak in the wavenumber range between 3100 cm^{-1} and 3700 cm^{-1} [19]. These features are present in all the samples, regardless of the surface modification, and indicate that the silanization process did not change the basic particle surface chemistry.

Besides the above peaks, the silane-modified DE particles show the presence of IR peaks at 2929 cm^{-1} attributed to -CH_2− asymmetric stretching and 2869 cm^{-1} attributed to -CH symmetric stretching[25], in good agreement with the presence of the carbon alkyl chains corresponding to the hydrophobic silanes. The relatively higher amplitudes of the -CH_2− and -CH peaks in the order of C18, C8, and C4 is in good agreement with the increasing length, and hence carbon content, of the alkyl chains used for surface modification. As expected, DE sample did not show the IR peaks related to the alkyl chain.

Effect of surface modification on loading and release of organic inhibitors in DE microparticles

Figure 4a–c show loading and release kinetics as a function of the surface modification calculated as indicated in Section 2.4. The overall loading of KDMTD corrosion inhibitor, as shown in Fig. 4a, increased for DE samples modified with longer alkyl chains (C8 and C18) compared to unmodified DE, while the C4-modified sample showed a decrease in overall loading. This overall trend can be explained by the differences in absorbed and adsorbed loading states.

The absorbed loading (blue column related to absorbed inhibitor in Fig. 4a) decreased across all silanized DE samples, indicating that surface modification generally reduced the absorption (i.e., less KDMTD in the container). This is attributed to the hydrophobic nature of silanized DE particles decreasing (bulky) inhibitor absorption on the DE outershell in water. On the other hand, the adsorbed loading (orange bars in Fig. 4a) increased significantly when longer alkyl chains were used (C8@DE-KDMTD and C18@DE-KDMTD), particularly in comparison to unmodified DE-KDMTD. This is attributed to the higher attractive forces between the alkyl chains on the DE surfaces and the DMTD organic ions than between -OH on the DE unmodified surfaces and the DMTD in presence of water, where DMTD needs to compete with surrounding H_2O molecules adsorbing on the DE surface, as illustrated in Fig. 4d. In agreement with this, the effect is more predominant when C8 and C18 alkyl silanes are used than when C4 alkyl chain was used. In the case of C8@DE-KDMTD and C18@DE-KDMTD the silanes create relatively thick hydrophobic zones that favour the presence of less polar DMTD (ionic state) over polar water molecules through diffusion. The comparable adsorption between the two was likely due to the coiling effect of the longer C18 silane chains slightly limiting the further expansion of the hydrophobic zone in the presence of water compared to C8, as illustrated in Fig. 4d.

Figure 4b and c show the release kinetics of the corrosion inhibitor as a function of the DE surface treatment during 3 h of immersion in water and in 0.05 M NaCl water solution, respectively. As shown in Fig. 4a (blue and red dots within the columns), the presence of NaCl ions did not significantly increase the total inhibitor release after 3 h immersion for any sample compared to the absence of NaCl. Similarly, NaCl in solution did not have a major effect on the release kinetics profile as seen when comparing Fig. 4b and c. This suggests release was dominated by rapid water dissolution and internal diffusion in the particles, while ion charge balance does not play a measurable role as opposite to other reported loading systems[34].

When attending at the release kinetics profile, the surface modification had a clearer effect as observed in Figs. 4a–c. The release profile of the DE-KDMTD particles without surface modification plateaued at around 45 minutes at 80% release fraction of the maximum theoretical release calculated based on the loading. The surface-modified C4, C8 and C18 DE-KDMTD particles showed a slower release profile and lower relative release fraction at the end of the experiment (3 h) than the DE particles. In spite of this lower release, the total inhibitor released for the same particle amount was comparably high for DE-KDMTD, C8@DE-KDMTD and C18@DE-KDMTD and lower for the C4@DE-KDMTD samples (blue and red dots in Fig. 4a). The samples modified with C4 silane showed a comparable release profile (kinetics and plateau at 60 min immersion) to the DE-KDMTD sample yet plateauing at 65% release fraction. The samples modified with the C8 and C18 silanes showed slower

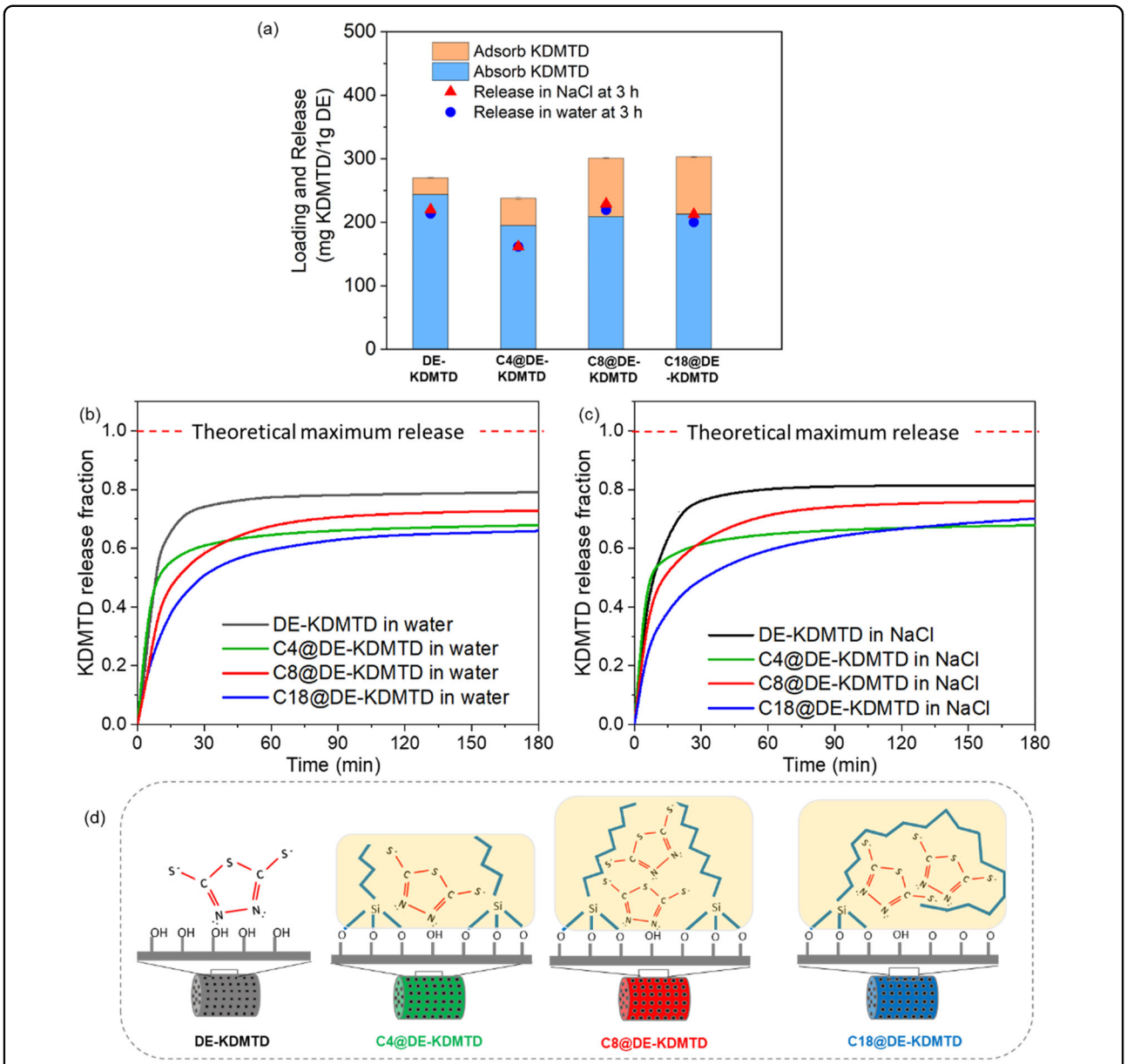

Fig. 4 Influence of surface modification on the loading and release of KDMTD corrosion inhibitor in DE particles. a Loading and release of KDMTD corrosion inhibitor in the DE particles as a function of the surface modification; **b** and **c** Fractional release kinetics of KDMTD corrosion inhibitor as a function of the surface modification in distilled water (**b**) and in 0.05 M NaCl aq. solution **c**. Theoretical maximum release is given by the total loading shown in Fig. 4a. **d** Schematic describing the loading principle of KDMTD corrosion inhibitor as a function of the DE surface modification. The yellow blocks indicate the hydrophobic zones governed by the alkyl chains.

release kinetics profiles, plateauing at around 90 min for the C8@DE-KDMTD and with no clear plateau for the C18@DE-KDMTD sample even at the end of the immersion time (3 h). This slower release rate can be explained by the hydrophobic character of the surface modification and is expected to be beneficial for corrosion protection as it combines a fast initial release of inhibitor with a sustained release in time, while no modification of the surface led just to a rapid release of inhibitor in the first minutes of immersion. While C4@DE-KDMTD did not seem to have a big impact on the release rate, the interactions between the inhibitor and surface modification may have affected the total inhibitor released in a comparable manner to the surface modification with C8 and C18. Nevertheless, more inhibitor molecules can be stored when the more hydrophobic silanes are used, as shown in Fig. 4d and discussed above, which in turn affects the diffusion kinetics of the adsorbed inhibitors. As expected, long carbon chains (C18) may collapse in water media and decrease release kinetics when compared to

C8@DE-KDMTD. This may also affect the total amount of inhibitor released in the studied time of 3 h (C8@DE-KDMTD 75% at 3 h, yet with C18@DE-KDMTD < 70%). Considering the requirements for corrosion inhibitor loading (as high as possible) and release (sufficient amount quickly released to rapidly protect the metal and then sustained release in time for maintenance of the protective layer), the C8 surface modified particles perform the best amongst the surface modified ones as they combine high loading (almost 3 fold the adsorbed inhibitor than DE-KDMTD), faster release behaviour amongst the surface modified ones and higher inhibitor fraction released (75%). For this reason, in the remaining part of the work, it was decided to compare the behaviour between coatings loaded with DE-KDMTD and C8@DE-KDMTD particles.

Effect of surface modification on particle dispersion in the coating

Figure 5a shows representative confocal microscope images of the coatings prepared with 30% PVC DE-KDMTD and C8@DE-KDMTD microparticles. In both coatings, the particles appeared to be well dispersed in the absence of large (>100 μm) agglomerates. Nevertheless, the particles modified with C8 alkyl silane showed a clear improvement in particle dispersion, with individual DE particles clearly identifiable (Fig. 5a-right).

Figure 5b shows SEM/EDS micrographs of the epoxy coatings containing DE-KDMTD and C8@DE-KDMTD after wet-grinding. In agreement with the confocal images, both coatings showed homogeneous particle distributions without agglomerates over the entire coating surface, even though the particles modified with C8(OTS) were more clearly identifiable and presented an even more homogeneous dispersion. When looking at the particles a bit closer (Fig. 5b), it became clear that the inner volume of the DE particles without silane modification was completely filled by organic matter (elemental C map) attributed to the epoxy-amine matrix, in good agreement with our previous reports with such DE-loaded coatings[35]. Quite opposite to this, the C8@DE-KDMTD particles appeared empty after polishing. This is attributed to a

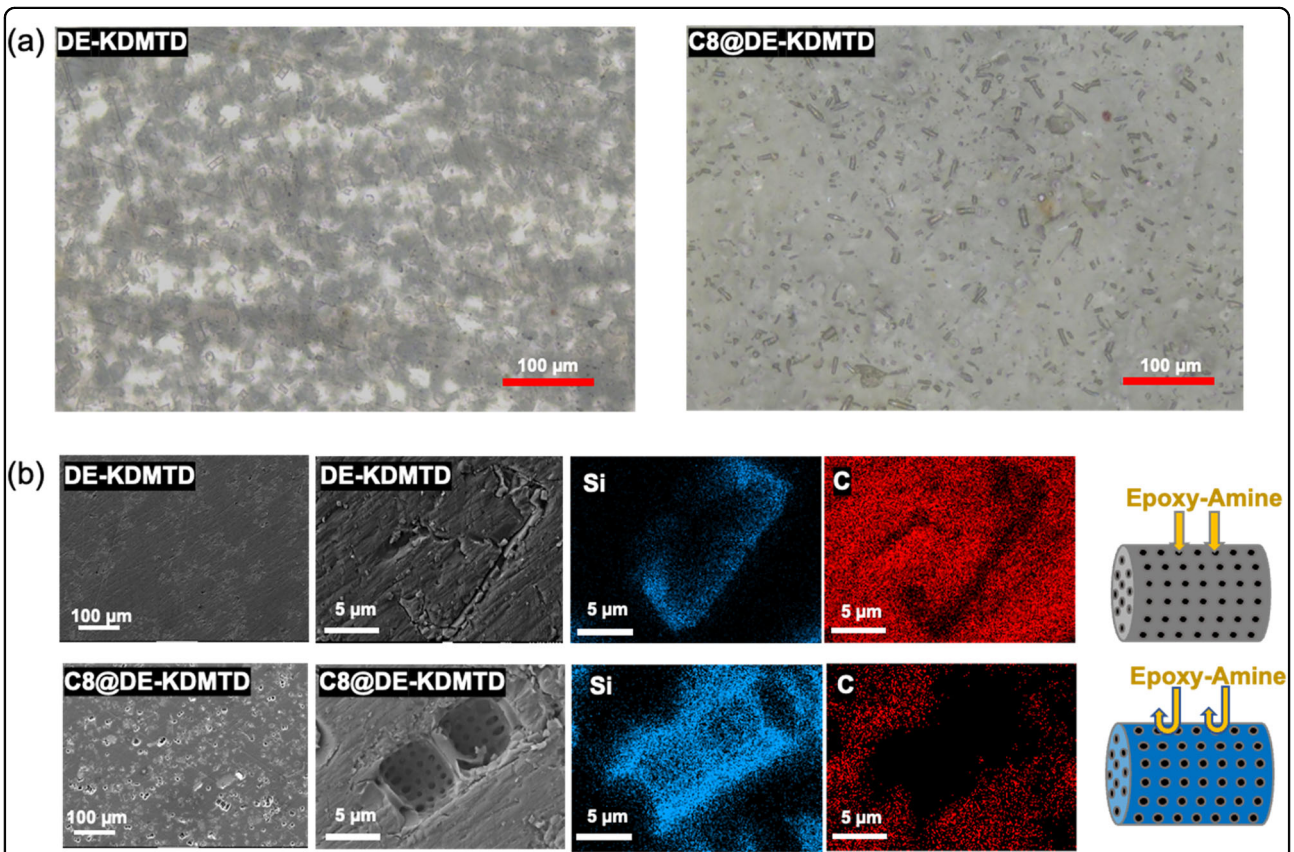

Fig. 5 Microscopic and elemental analysis of coatings containing DE-KDMTD and C8@DE-KDMTD particles. a Confocal microscope images of as-prepared coatings with DE-KDMTD and C8@DE-KDMTD particles; **b** SEM-EDX analysis of wet-ground coatings containing DE-KDMTD and C8@DE-KDMTD particles. EDX is unable to detect the presence of KDMTD because it can be dissolved during the wet grinding process. The images show how the C8 treatment help decrease the penetration of the epoxy-amine resin into the DE particles as opposed to the DE-KDMTD particles, as shown in the right scheme.

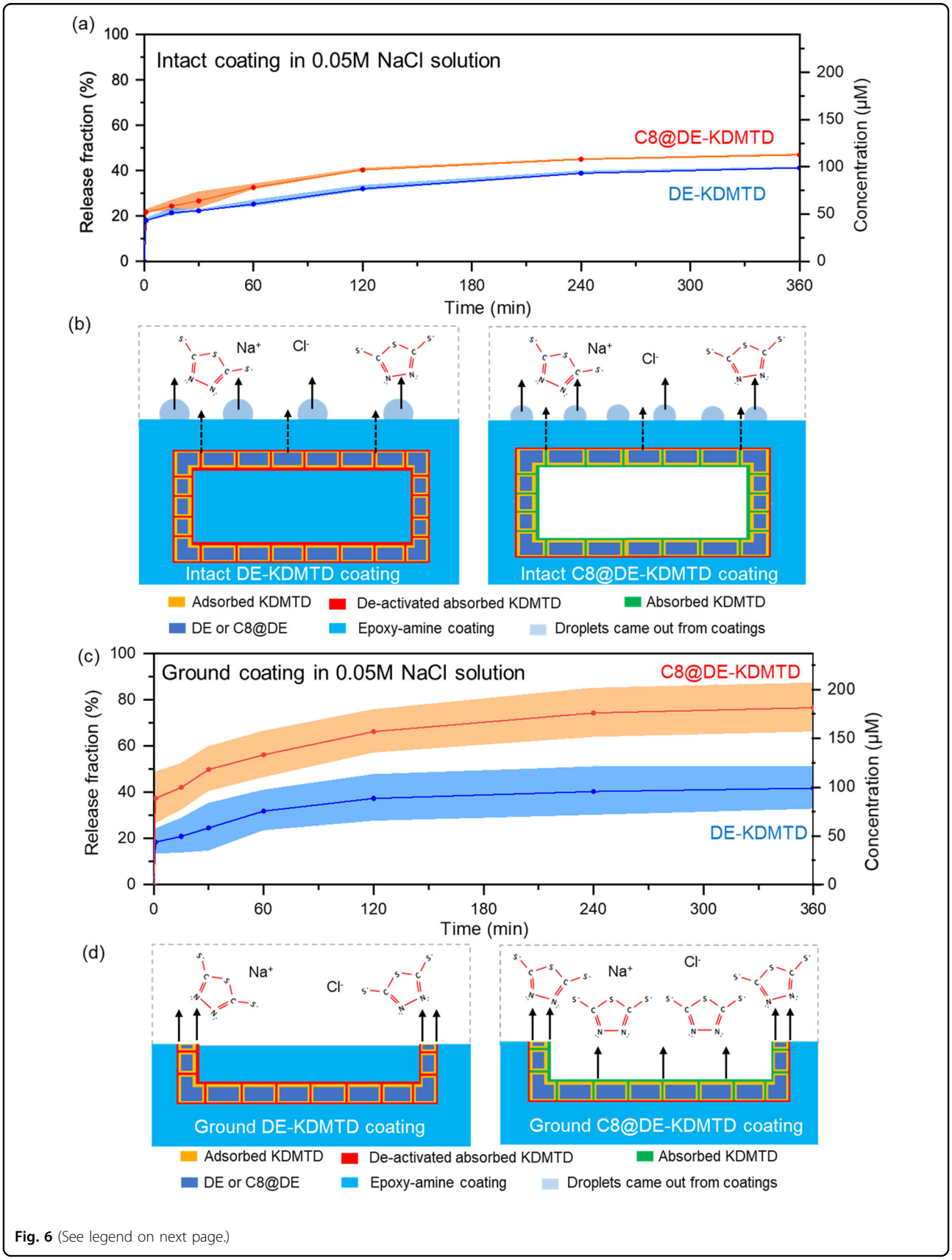

Fig. 6 (See legend on next page.)

(see figure on previous page)
Fig. 6 Release behavior of KDMTD from coatings containing DE-KDMTD and C8@DE-KDMTD particles in 0.05 M NaCl solution. Release profiles from coatings containing DE-KDMTD and C8@DE-KDMTD particles exposed to 0.05 M NaCl solution over 6 h using as-produced intact coatings (**a**) and dry-ground coatings (**c**). Shadow regions represent deviation between repeats. Schemes **b** and **d** show representations of KDMTD inhibitor release from intact coatings, where the diatomite structure is covered by epoxy-amine coating binder (**b**), and ground coatings, where the diatomite shell structures are exposed to the solutions (**d**). Blue semi-spheres at the coating surface represent initial inhibitor exudation leading to

barrier effect induced by the silane surface modification that ensured epoxy-amine polymerization at the surface and prevented it from getting into the DE inner volume, as also shown in the EDX mapping.

Effect of surface modification on inhibitor release from coatings

The effect of DE surface modification on the release of KDMTD from the coatings was investigated by exposing the coatings as-produced (Fig. 6a) and the coatings after grinding (Fig. 6b) to 0.05 M NaCl solutions and monitoring DMTD concentration in solution with UV-Vis spectroscopy. The release fraction was calculated by dividing the "inhibitor concentration released into the container above the coating" by the "maximum inhibitor concentration that can be released from the coating beneath the container." This calculation takes into account the PVC used and the estimated inhibitor loading in the particles. As seen in Fig. 6, the release takes place in two stages independently of the diatomite surface treatment and the coating surface condition (ground or intact), namely: (i) very fast initial release right after exposure to electrolyte, followed by (ii) sustained release until 2 or 6 h, depending on the sample. In all cases, higher release fractions and total inhibitor release were observed when C8 surface modification of the diatomite shell was used.

In the case of intact coatings (Fig. 6a), the initial fast release fraction is quite comparable (~20%), independently of the surface treatment of the diatomite carrier. A close look at the intact coating surfaces exposed to air for 1 day, unveiled the presence of droplets at the coating surface, as shown in the optical images in the left column in Fig. 7 and illustrated in Fig. 6b. These exudate droplets were attributed to the hygroscopic character of KDMTD. Despite the similar exhumation phenomena in both coatings, the droplets on the C8@DE-KDMTD coating were smaller than those on DE-KDMTD coating highlighting the beneficial effect of the hydrophobic nature of the modified carriers. We hence attribute the initial fast release from intact coatings right after immersion to this exudation phenomena. Important to notice is that, after 2 h immersion in NaCl solution, drying and exposure to air for 1 day, no exudates were detected anymore as shown in the right images in Fig. 7.

Due to the surface grinding before immersion, the effect of the exudates is not considered the main responsible for the fast initial release observed in the ground coatings (Fig. 6c). Interestingly, the ground DE-KDMTD coating shows comparable initial release as its intact counterpart (~20%), while the coating with C8@DE-KDMTD particles shows 2 times more initial release (~40%). Considering the comparable inhibitor loading in the particles (Fig. 4) and the good dispersion in both coatings (Fig. 5), we attribute the higher released fraction in the case of the C8@DE-KDMTD particles to the positive effect of the surface treatment in isolating the inhibitor from the surrounding polymer matrix. This protection leads to lower resin penetration in the DE particles modified with C8 alkyl silane (Fig. 5 and scheme in Fig. 6d) and therefore approximately 2 times more unreacted inhibitor is readily available to be released upon exposure to the electrolyte.

Following the initial relatively fast release, the release of the two intact coatings (Fig. 6a) gradually increased and reached a plateau at 2 h, with a final release fraction of up to 48% for C8@DE-KDMTD and 40% for DE-KDMTD. This similar release amount suggests that inhibitor diffusion from the inner coating to the surface in intact coatings mostly happens during the first 2 h immersion, possibly being limited due to local swelling closing diffusion paths in the intact polymer coating at the top surface. Interestingly, a similar release profile with comparable final release fraction and amount was found for the DE-KDMTD coating after grinding. This is attributed to a predominant release of absorbed KDMTD in the coating regions closer to the surface, largely influenced by diffusion through the polymer binder.

Clearer differences between intact and ground coatings are found for the coatings containing C8@DE-KDMTD particles. When surface ground, these coatings showed a consistently higher release rate and release fraction during the 6 h immersion test. At the end of the 6 h, around 80 to 90% fraction of the available inhibitor was released without reaching a release plateau. This significantly higher release fraction (around 35% more than for the DE-KDMTD coating) can be attributed to the significantly lower negative reactions between the organic inhibitor and the surrounding polymeric matrix when using the octyl alkyl silane surface treatment of the diatomite

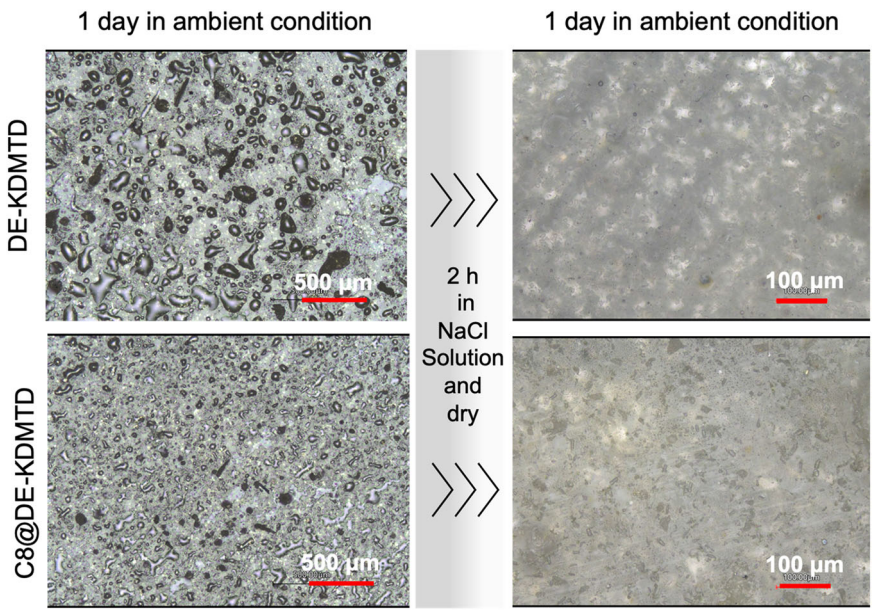

Fig. 7 Confocal microscopy images of the intact coatings containing DE-KDMTD and C8@DE-KDMTD particles. Images were taken after 1 day of exposure to ambient conditions (left column) and after exposure to NaCl solution for 2 hours, followed by drying and an additional 1 day exposure to ambient conditions (right column).

particles. It is therefore hypothesized that the surface modification in the C8@DE particles acts as a loading layer (Fig. 4d) but also as a protective layer that prevents the epoxy matrix from penetrating into the DE particles and reacting with KDMTD. As a consequence, higher amounts of KDMTD are readily available to be released when the surface-modified particles are used. Overall, these results suggest that a higher corrosion inhibition efficiency would be expected for the coatings containing C8 surface-modified DE particles loaded with KDMTD, as addressed in the following section.

Effect of surface modification on active corrosion protection at damaged coatings

Figure 8a–c show surface activity maps, surface activity coverage with time, and post-mortem micrographs of the damages for the coatings containing DE-KDMTD and C8@DE-KDMTD particles exposed to pH 7 0.05 M NaCl solution for 2 h, moment at which most of the releasable KDMTD should have been released based on release tests (Fig. 6). Figure 8d shows the absorbance peak of the solutions at 2 h related to KDMTD release. As shown in Fig. 8a, the local activity at the damage location for the coating with DE-KDMTD started short after immersion (black curve in Fig. 8a starting to rise at around 5 min), then increasing to 45% surface coverage within 1 h and 64% surface coverage at 2 h, when it started plateauing. This activity was identified as (minimal) corrosion-related activity. This was confirmed with the post-mortem imaging revealing dealloying and trenching (Fig. 8b) even if lower than expected for unprotected coatings or coatings using DMTD directly added to the coating[11]. The coating with KDMTD loaded in C8@DE showed significantly lower surface activity coverage and kinetics (Fig. 8b) and intensity of activity (Fig. 8a) identified by the histogram colours at the metal surface being mostly yellow-red rather than purple as in the case of DE-KDMTD). The imaged dynamic process stabilizes (surface activity plateaus) at 1.5 h and reaches 25% surface coverage at significantly lower intensity levels. Post-mortem images confirmed that the extent of localized corrosion was significantly lower than for the DE-KDMTD samples (Fig. 8c). Moreover, a UV-Vis analysis of the aliquots at 2 h (Fig. 8d) showed there was 21% more KDMTD released from the damaged C8@DE-KDMTD coating than from the DE-KDMTD coating ($1.6{\cdot}10^{-4}$ vs $1.3{\cdot}10^{-4}$ M). Despite the clear improvement in KDMTD release when using C8@DE particles, in both cases, the levels of inhibitor released are lower, especially during the first 60 min immersion, than the inhibitor concentration threshold necessary to fully stop the initial dealloying of intermetallic particles occurring within the first 5-10 min immersion[23,36]. Nevertheless, the continuous inhibitor release during immersion allowed stopping the dealloying and trenching process, reflected in a plateau in the surface activity% % and activity intensity map at 1.5 h immersion for the case of the coating containing C8@DE particles.

In previous works, we demonstrated that one of the factors responsible for the high levels of corrosion protection offered by an inhibitor related to KDTMD, namely

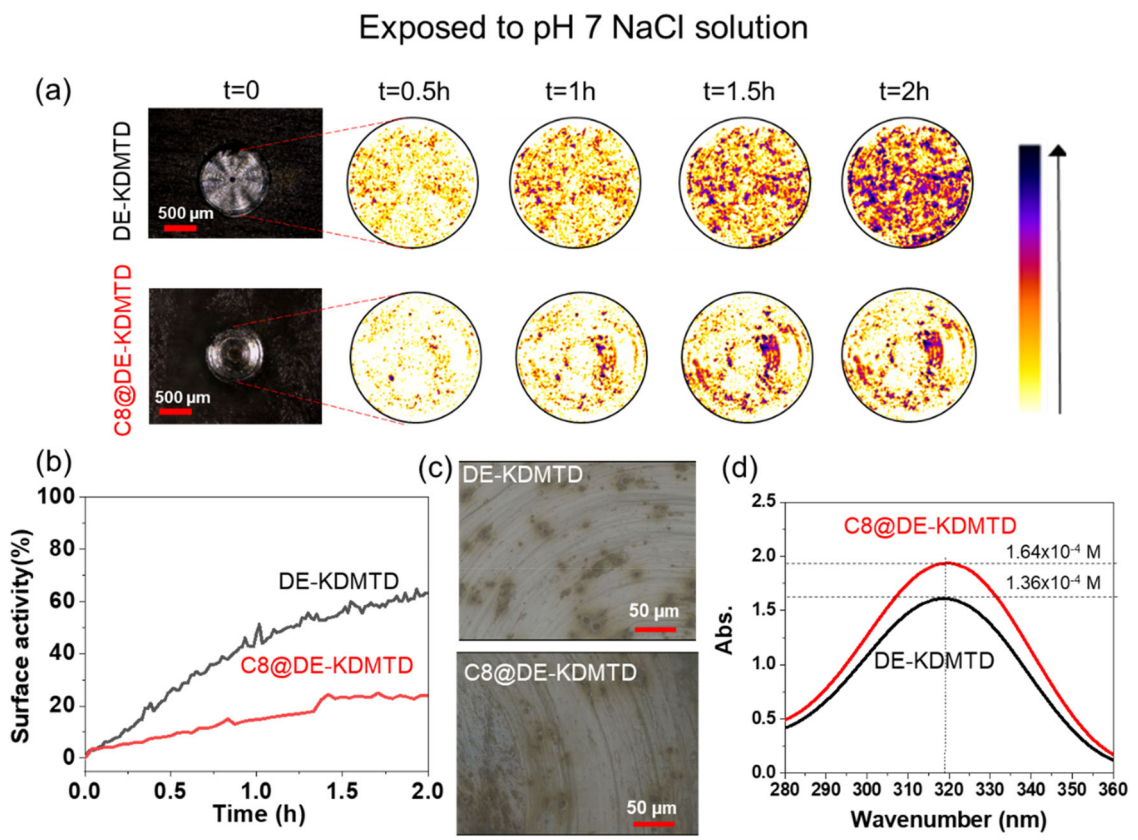

Fig. 8 Corrosion activity and inhibitor release in damaged coatings containing DE-KDMTD and C8@DE-KDMTD particles under exposure to pH 7 NaCl solution. a Optical images at t = 0 with global activity maps at selected immersion times. Colour bar shows the intensity histogram of the local changes with black being changes of higher intensity with respect to image at time 0; **b** time evolution of the activity surface coverage in %; **c** local post-mortem micrographs of the damage; and **d** UV-Vis spectra of the electrolyte at the end of the 2 h exposure in pH 7 NaCl solutions of damaged coatings containing DE-KDMTD (black lines) and C8@DE-KDMTD (red lines). The diameter of the damage hole is 1 mm.

HDMTD, is its natural acidity (leading to pH = 2 in starting neutral solutions)[11,17]. Different to HDMTD, KDMTD salt studied in this work leads to a natural neutral pH. In order to study the benefit of an acidic environment in the corrosion inhibition potential of coatings loaded with KDMTD, the active protection at damaged coatings exposed to pH 5 was evaluated. As shown in Fig. 9a and c, when the damaged coatings were exposed to pH 5, no relevant signs of surface activity was observed during the whole immersion time. This indicates a full degree of protection in both coatings, as confirmed by the post-mortem analysis shown in Fig. 9c. Notably, the post-mortem solutions at pH 5 exhibited a higher absorbance wavelength (326 nm) than those exposed at neutral pH (320 nm) as shown in Fig. 9d. This shift in wavenumber indicates a high degree of inhibitor deprotonation when exposed to more acidic pH[23,37,38], factor that, together with the removal of the natural aluminium oxide layer leads to higher inhibitor adsorption and high degrees of protection as also observed with HDMTD in initially neutral solutions[23].

Effect of surface modification on inhibiting layer stability: wet-dry cyclic tests

As highlighted in our previous works[11,23], inhibitor layer stability during re-exposure appears as a major, yet largely unattended, factor to consider when developing anticorrosive coatings. Figure 10 shows the effect of sequentially re-exposing to neutral NaCl solution the damaged coatings first exposed to pH 5 shown in Fig. 9; i.e. exposure to pH 5 + drying + 1st re-exposure to pH 7 + drying + 2nd re-exposure to pH 7.

Upon first re-exposure to pH 7 NaCl solution (as shown in Fig. 10a–d), the C8@DE-KDMTD coating continued to exhibit negligible surface activity at the damaged site, whereas the DE-KDMTD coating showed initial local activity that stabilized at around 2.5% surface coverage within 5 minutes of exposure. This aligns with the post-mortem imaging suggesting slight dealloying at some local intermetallic particles for the DE-KDTMD sample (Fig. 10c). Remarkably, the detected activity phenomena occurring at the intermetallic particles stopped after the initial 5 min of immersion. A UV-Vis analysis of the

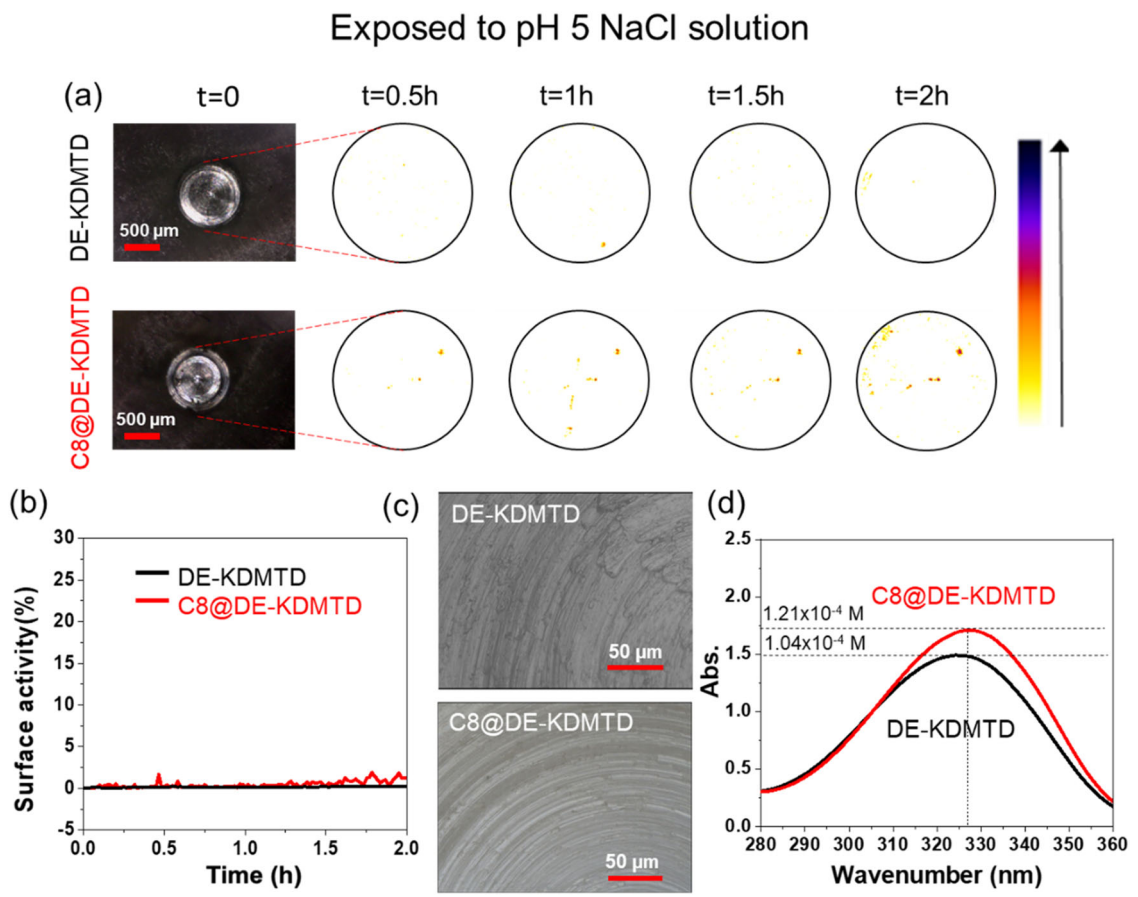

Fig. 9 Corrosion activity and inhibitor release in damaged coatings containing DE-KDMTD and C8@DE-KDMTD particles under exposure to pH 5 NaCl solution. a Optical images at $t = 0$ with global activity maps at selected immersion times. Colour bar shows the intensity histogram of the local changes with black being changes of higher intensity with respect to image at time 0; **b** time evolution of the activity surface coverage in %; **c** local post-mortem micrographs of the damage; and **d** UV-Vis spectra of the electrolyte at the end of the 2 h exposure in pH 5 NaCl solutions of damaged coatings containing DE-KDMTD (black lines) and C8@DE-KDMTD (red lines). The diameter of the damage hole is 1 mm.

electrolyte (Fig. 10d) revealed a good amount of inhibitor being released during re-exposure (~10^{-5}M). It is hypothesized that this continued inhibitor release during reimmersion contributed to the stabilization of the inhibiting layer initially created during the first immersion, despite the initial destabilization induced by the neutral pH exposure. In contrast with this initial (small) activity, the sample with C8@DE-KDMTD particles showed no local activity (Fig. 10a–c). This is in good agreement with the relatively high amount of inhibitor being released (~3×10^{-5}M and 3 times higher than for DE-KDMTD), leading to very efficient inhibiting layer stabilization. In any case, both systems showed significant robustness of the protective system in the event of a wet-dry-wet cycle.

A more noticeable difference between the two coatings emerged during the second re-exposure event (Fig. 10e–h). During this second re-immersion, the coating with non-modified particles (DE-KDMTD coating) exhibited immediate surface activity propagating at a surface coverage propagation rate of 17% h^{-1} and stabilizing at 25% surface activity after 1.5 h exposure. Interestingly, the surface analysis showed large optical fluctuations, which, considering the relatively reduced local corrosion extension observed in the micrograph (Fig. 10g), may be attributed to the continuous destabilization and stabilization of the inhibiting layer due to extra inhibitor supply. This suggests that the inhibiting layer formed during immersion was unstable with the immersion time (total of 6 h) and/or that the inhibitor release at similar amounts as in the first re-immersion (Fig. 10a) was insufficient to fully counterbalance the instability of the inhibiting layer at pH 7 for this sample.

In contrast to the DE-KDMTD coating, the coating loaded with C8@DE-KDMTD particles showed significantly better results with: (i) a delayed onset of surface activity (detectable surface activity starts after 15 min immersion); (ii) a surface activity propagation rate significantly lower (6.4% h^{-1}) and at significantly lower

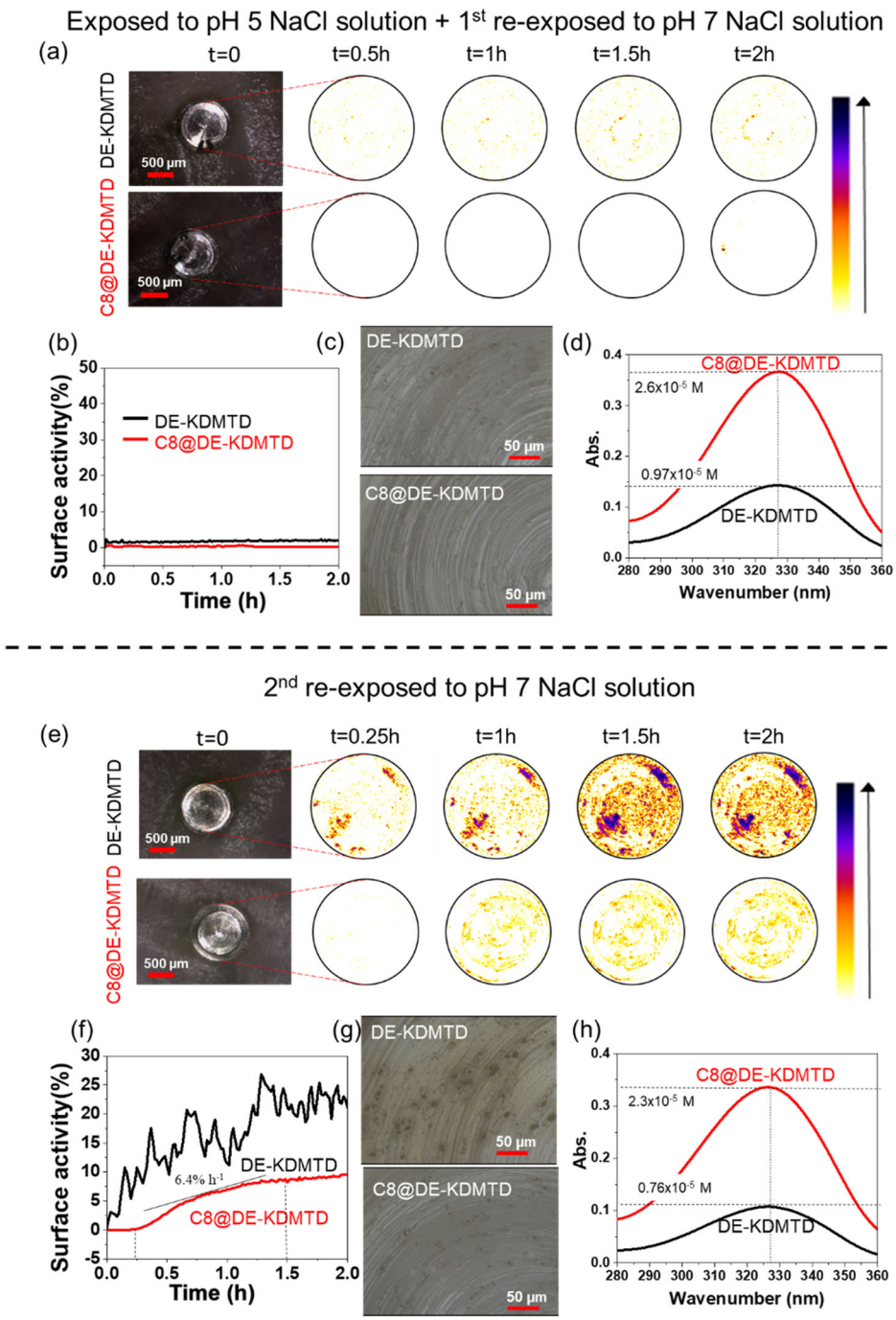

Fig. 10 Corrosion activity and inhibitor release in damaged coatings containing DE-KDMTD and C8@DE-KDMTD particles under sequential re-exposures. Optical images at $t = 0$, global activity maps at selected immersion times, time evolution of surface activity and related intensity histogram, local post-mortem confocal microscopic images of the damage, and UV-Vis spectra of the electrolyte at the end of the 2 h exposure in pH 5 NaCl solutions of damaged coatings containing DE-KDMTD (black lines) and C8@DE-KDMTD (red lines) exposed to pH 5 NaCl solution, following by **a**–**d** 1st re-exposed to pH 7 NaCl solution and **e**–**h** 2nd re-exposed to pH 7 NaCl solution. The diameter of the damage hole is 1 mm.

intensity (yellow colour activity instead of the purple); (iii) a rapid end of the surface activity progression after 1.5 h immersion at a low surface coverage of 9%; and (iv) the absence of noise in the activity progression. The postmortem analysis confirmed the surface activity was related to very reduced localized activity at some intermetallic particles (Fig. 10g). Interestingly, also in this case, the amount of inhibitor released was similar to the

amounts measured during the first re-exposure test (2.5×10^{-5} M, being 3 times higher than for the DE-KDMTD sample, Fig. 10h) and points at a threshold concentration of inhibitor needed to maintain the full stability of the inhibiting layers formed at first instance at pH 5; which are intrinsically more stable when more inhibitor is released in the first instance (i.e. first immersion step). Interestingly, the release amounts during the second re-exposure for the C8@DE-KDMTD coating is comparable to our previous work using HDMTD particles protected by a thin nano-layer deposited by CVD in fluidized bed (2.5×10^{-5} M during re-exposure)[11]. In the concept here presented using diatomite as carrier, this threshold of inhibitor being released during re-immersions (1×10^{-5} M < [inhibitors] <2.3×10^{-5} M) can better be better supported when using a C8 alkyl silane surface treatment due to the improved loading and the improved protection of the loaded inhibitor from the surrounding matrix.

The results and hypothesis discussed above are summarized in Fig. 11, for the coatings with DE-KDMTD and C8@DE-KDMTD particles when exposed to pH 7 0.05 M NaCl solution (a), and pH 5 0.05 M NaCl solution followed by two subsequent exposures to pH 7 0.05 M NaCl solution (b). DE-KDMTD and C8@DE-KDMTD particles show slightly different degrees of dispersion (better dispersion for C8-modifed particles). More relevantly, while particles without any surface modification are filled with the polymer binder leading to some degree of reaction and immobilization of the loaded KDMTD, the alkyl silane surface modification (OTS) prevents resin infiltration in the diatomite shell resulting in the presence of empty particles well dispersed in the coating (as shown in Fig. 5). Consequently, more inhibitors remain protected from the surrounding matrix and therefore active and ready to be quickly released at damaged locations.

When exposed to a pH 7, 0.05 M NaCl solution (Fig. 11a), a significant improvement in KDMTD release

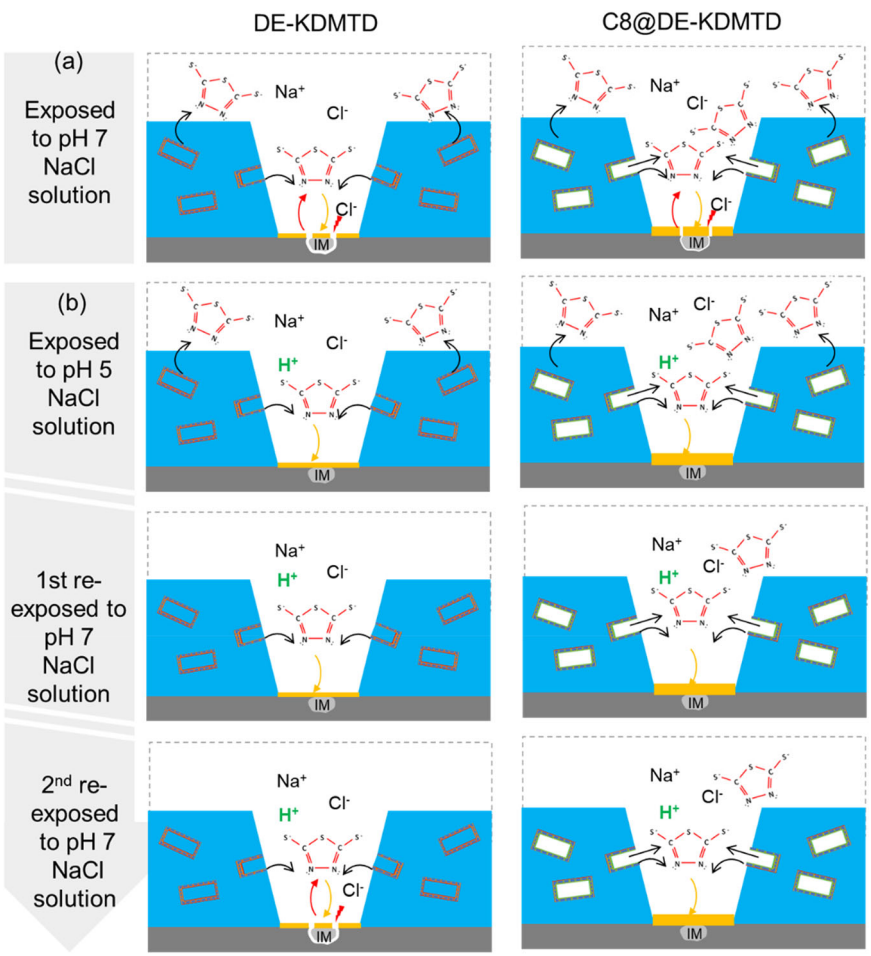

Fig. 11 Schematic illustration of the damaged coatings containing DE-KDMTD and C8@DE-KDMTD particles under different exposure conditions. a pH 7 0.05 M NaCl solution, and **b** pH 5 0.05 M NaCl solution followed by two subsequent exposures to a pH 7 0.05 M NaCl solution. The continuous supply of inhibitor beyond a critical level as achieved by C8(OTS) surface modification allows sustaining the inhibiting layer efficiently protecting the exposed metal surface.

and corrosion inhibition was observed if C8@DE particles were used. This improvement was attributed to better particle dispersion, storage of inhibitor in the alkyl layer, and the prevention of resin penetration in the carrier. However, the initial dealloying and trenching corrosion could not be completely avoided as attributed to the relatively reduced inhibitor release and, more importantly, the complex ionic state of KDMTD limiting its efficiency.

In contrast, despite the particle dispersion and resin infiltration differences, both coatings show high levels of protection at damage sites when coatings are exposed to pH 5 0.05 M NaCl solution (Fig. 11b), even though a more stable protective layer is still formed in the C8@DE-KDMTD coating attributed to a higher inhibitor release (Fig. 9d). Upon re-exposure to pH 7 NaCl solution, both damaged areas remain well-protected, likely related to the robust stability of the inhibiting layer on the metal and a sufficient resupply of inhibitor to maintain inhibiting layer stability (Fig. 10d). During the second re-exposure to pH 7 NaCl solutions, the DE-KDMTD partially lost its effective protection attributed to a limited supply of inhibitor estimated to be below a critical level to fully maintain inhibiting layer stability. The samples loaded with C8@DE-KDMTD particles on the other hand showed full protection attributed to a very stable inhibiting layer further sustained by sufficient inhibitor release from the coating (approximately 3 times higher, Fig. 10h. The results indicate that a good isolation of the organic corrosion inhibitor from the surrounding matrix and an adequate inhibitor chemical state led to stable inhibiting layers offering high levels of protection, while sustained release beyond a critical level contributes sustaining high degrees of corrosion protection.

Conclusions

This study demonstrates that the loading and release of organic inhibitors from diatomite particles can be tuned using surface modification of the diatomite carriers with hydrophobic silanes. Of the three alkyl silanes used (BTS (C4), OTS (C8), and ODTS (C18)) the mid-length silane (OTS, C8) led to the best combination of higher inhibitor loading, 3.5 times higher inhibitor adsorption ratio than the reference non-modified diatomite, sustained release in time, and high inhibitor release fraction with respect to loading (70–75%).

When added to organic coatings, the C8-modified DE particles showed better particle dispersion within epoxy-amine matrices with minimal resin infusion into the hollow core of the diatomite particles. As a consequence, about 35% more inhibitor was available to protect damaged locations than without surface modification. Quantitative image reflectometry analysis during immersion showed slightly better protection at damaged sites (1 mm diameter) of the coatings using C8-modified particles when exposed to pH 7, even though minimal local corrosion attack in the first exposure stages was not completely stopped in either of the two coatings. At pH 5, both coatings showed excellent protection of the damage site with no apparent corrosion. Samples exposed to pH 5 and then re-exposed to pH 7, 0.05 M NaCl demonstrated very high stability of the inhibiting layers during the first re-immersion cycle of 2 h. In a second re-immersion step in neutral pH 0.05 M NaCl, the coatings loaded with unmodified diatomite slightly lost their highly protective efficiency, while the coatings loaded with C8 modified particles maintained very high levels of protection. This is attributed to the higher inhibiting layer stability and the improved continuous inhibitor supply facilitated by the inhibitor loading protection from the surrounding polymer matrix provided by the alkyl silane surface modification. This study demonstrates that organic corrosion inhibitors can be efficiently loaded into diatomite particles through surface modification to allow reduced negative interactions with the surrounding coating matrix and therefore offer enhanced and sustained protection at damaged locations, at least during three wet/dry cyclic exposure tests in the absence of delamination and blistering. Future studies with this technology will benefit from long-term cyclic exposure, neutral salt fog exposure, and overall coating performance with formulations closer to end-user coatings.

Acknowledgements

The authors acknowledge the financial support by Airbus Operations GmbH and Holland High Tech programme. The authors acknowledge Dr. Markus Jordan from Airbus Operations GmbH for his continued support and constructive discussions.

Author contributions

S.G. and J.Z. conceptualized the idea. D.N. performed surface modification, characterization, loading and release tests. J.Z. prepared and evaluated the coating and performed the corrosion protection tests. J.Z. and D.N. wrote the original draft. Every author reviewed and edited the manuscript. S.G. supervised all aspects of the research.

Conflict of interest

The authors declare no competing interests.

Received: 27 November 2024 Revised: 7 May 2025 Accepted: 19 May 2025
Published online: 20 June 2025

References

1. Sørensen, P. A., Kiil, S., Dam-Johansen, K. & Weinell, C. E. Anticorrosive coatings: a review. *J. Coat. Technol. Res.* **6**, 135–176 (2009).
2. Lyon, S. B., Bingham, R. & Mills, D. J. Advances in corrosion protection by organic coatings: What we know and what we would like to know. *Prog. Org. Coat.* **102**, 2–7 (2017).
3. Cui, G. et al. A comprehensive review on smart anti-corrosive coatings. *Prog. Org. Coat.* **148**, 105821 (2020).
4. Sinko, J. Challenges of chromate inhibitor pigments replacement in organic coatings. *Prog. Org. Coat.* **42**, 267–282 (2001).

5. Visser, P., Liu, Y., Terryn, H. & Mol, J. Lithium salts as leachable corrosion inhibitors and potential replacement for hexavalent chromium in organic coatings for the protection of aluminum alloys. *J. Coat. Technol. Res.* **13**, 557–566 (2016).
6. Rodič, P. & Milošev, I. Corrosion inhibition of pure aluminium and alloys AA2024-T3 and AA7075-T6 by cerium (III) and cerium (IV) salts. *J. Electrochem. Soc.* **163**, C85 (2015).
7. Lamaka, S. V., Zheludkevich, M. L., Yasakau, K., Montemor, M. & Ferreira, M. G. High effective organic corrosion inhibitors for 2024 aluminium alloy. *Electrochim. Acta* **52**, 7231–7247 (2007).
8. Obot, I., Macdonald, D. & Gasem, Z. Density functional theory (DFT) as a powerful tool for designing new organic corrosion inhibitors. Part 1: an overview. *Corros. Sci.* **99**, 1–30 (2015).
9. Zheludkevich, M., Tedim, J. & Ferreira, M. "Smart" coatings for active corrosion protection based on multi-functional micro and nanocontainers. *Electrochim. Acta* **82**, 314–323 (2012).
10. Denissen, P. J., Homborg, A. M. & Garcia, S. J. Requirements for corrosion inhibitor release from damaged primers for stable protection: a simulation and experimental approach using cerium loaded carriers. *Surf. Coat. Technol.* **430**, 127966 (2022).
11. Zhao, J., van Ommen, J. R. & Garcia, S. J. Gas-phase deposited nanolayers guard organic microparticles in polymer matrices for active corrosion protection at damages. *Prog. Org. Coat.* **192**, 108522 (2024).
12. Grigoriev, D., Akcakayiran, D., Schenderlein, M. & Shchukin, D. Protective organic coatings with anticorrosive and other feedback-active features: micro- and nanocontainers-based approach. *Corrosion* **70**, 446–463 (2014).
13. Altin, A., Rohwerder, M. & Erbe, A. Cyclodextrins as carriers for organic corrosion inhibitors in organic coatings. *J. Electrochem. Soc.* **164**, C128 (2017).
14. Kim, C., Karayan, A. I., Milla, J., Hassan, M. & Castaneda, H. Smart coating embedded with pH-responsive nanocapsules containing a corrosion inhibiting agent. *ACS Appl. Mater. interfaces* **12**, 6451–6459 (2020).
15. Abdullayev, E. & Lvov, Y. Clay nanotubes for corrosion inhibitor encapsulation: release control with end stoppers. *J. Mater. Chem.* **20**, 6681–6687 (2010).
16. Yabuki, A., Kanagaki, M., Nishikawa, C., Lee, J. H. & Fathona, I. W. Effective release of corrosion inhibitor by cellulose nanofibers and zeolite particles in self-healing coatings for corrosion protection. *Prog. Org. Coat.* **154**, 106194 (2021).
17. Shchukin, D. G. et al. Active anticorrosion coatings with halloysite nanocontainers. *J. Phys. Chem. C.* **112**, 958–964 (2008).
18. Olivieri, F., Castaldo, R., Cocca, M., Gentile, G. & Lavorgna, M. Mesoporous silica nanoparticles as carriers of active agents for smart anticorrosive organic coatings: a critical review. *Nanoscale* **13**, 9091–9111 (2021).
19. Borisova, D., Akçakayıran, D., Schenderlein, M., Möhwald, H. & Shchukin, D. G. Nanocontainer-based anticorrosive coatings: effect of the container size on the self-healing performance. *Adv. Funct. Mater.* **23**, 3799–3812 (2013).
20. Snihirova, D., Lamaka, S. V. & Montemor, M. SMART" protective ability of water based epoxy coatings loaded with CaCO3 microbeads impregnated with corrosion inhibitors applied on AA2024 substrates. *Electrochim. Acta* **83**, 439–447 (2012).
21. Denissen, P. J., Shkirskiy, V., Volovitch, P. & Garcia, S. J. Corrosion inhibition at scribed locations in coated AA2024-T3 by cerium-and DMTD-loaded natural silica microparticles under continuous immersion and wet/dry cyclic exposure. *ACS Appl. Mater. interfaces* **12**, 23417–23431 (2020).
22. Denissen, P. J. & Garcia, S. J. Cerium-loaded algae exoskeletons for active corrosion protection of coated AA2024-T3. *Corros. Sci.* **128**, 164–175 (2017).
23. Zhao, J., Santoso, A. & Garcia, S. J. Small concentrations of NaCl help building stable inhibiting layers from 2, 5-dimercapto-1, 3, 4-thiadiazole (DMTD) on AA2024-T3. *Corros. Sci.* **225**, 111562 (2023).
24. Mahtabani, A. et al. Gas phase modification of silica nanoparticles in a fluidized bed: Tailored deposition of aminopropylsiloxane. *Langmuir* **37**, 4481–4492 (2021).
25. Bariana, M., Aw, M. S., Kurkuri, M. & Losic, D. Tuning drug loading and release properties of diatom silica microparticles by surface modifications. *Int. J. Pharm.* **443**, 230–241 (2013).
26. Aw, M. S., Bariana, M., Yu, Y., Addai-Mensah, J. & Losic, D. Surface-functionalized diatom microcapsules for drug delivery of water-insoluble drugs. *J. Biomater. Appl.* **28**, 163–174 (2013).
27. Bariana, M., Aw, M. S. & Losic, D. Tailoring morphological and interfacial properties of diatom silica microparticles for drug delivery applications. *Adv. Powder Technol.* **24**, 757–763 (2013).
28. Kumeria, T. et al. Graphene oxide decorated diatom silica particles as new nano-hybrids: towards smart natural drug microcarriers. *J. Mater. Chem. B* **1**, 6302–6311 (2013).
29. Li, H. et al. Functionalized silica nanoparticles: classification, synthetic approaches and recent advances in adsorption applications. *Nanoscale* **13**, 15998–16016 (2021).
30. Bremmell, K. E. & Prestidge, C. A. Enhancing oral bioavailability of poorly soluble drugs with mesoporous silica based systems: Opportunities and challenges. *Drug Dev. Ind. Pharm.* **45**, 349–358 (2019).
31. Yu, Y., Addai-Mensah, J. & Losic, D. Functionalized diatom silica microparticles for removal of mercury ions. *Sci. Technol. Adv. Mater.* **13**, 015008 (2012).
32. Sheng, G. et al. Adsorption of Pb (II) on diatomite as affected via aqueous solution chemistry and temperature. *Colloids Surf. A: Physicochem. Eng. Asp.* **339**, 159–166 (2009).
33. Sheng, G., Hu, J. & Wang, X. Sorption properties of Th (IV) on the raw diatomite—effects of contact time, pH, ionic strength and temperature. *Appl. Radiat. Isotopes* **66**, 1313–1320 (2008).
34. Peng, Y. et al. Leaching behavior and corrosion inhibition of a rare earth carboxylate incorporated epoxy coating system. *ACS Appl. Mater. interfaces* **11**, 36154–36168 (2019).
35. Denissen, P. J., Shkirskiy, V., Volovitch, P. & Garcia, S. J. Corrosion Inhibition at Scribed Locations in Coated AA2024-T3 by Cerium- and DMTD-Loaded Natural Silica Microparticles under Continuous Immersion and Wet/Dry Cyclic Exposure. *ACS Appl Mater. Interfaces* **12**, 23417–23431, https://doi.org/10.1021/acsami.0c03368 (2020).
36. Mopon, M. Jr, Mol, A. & Garcia, S. J. Effect of delayed inhibitor supply on AA2024-T3 intermetallic activity: A local in situ analysis with reflected microscopy. *Corros. Sci.* **230**, 111910 (2024).
37. Stanovnik, B. & Tišler, M. Contribution to the Structm· e of 2, 5-Dimercapto-1, 3, 4-thiadiazole and related compounds. *Croatica Chem. Acta* **37**, 17–23 (1965).
38. Galvão, T. L. et al. A computational UV–Vis spectroscopic study of the chemical speciation of 2-mercaptobenzothiazole corrosion inhibitor in aqueous solution. *Theor. Chem. Acc.* **135**, 1–11 (2016).